

# $sp^3$ domain in graphite by visible light and photoinduced phase transitions

K. Nasu<sup>a</sup>

Solid State Theory Division, Institute of Materials Structure Science, KEK, Graduate University for Advanced Study and CREST JST, 1-1, Oho, Tsukuba, 305-0801, Japan

Received 5 January 2010 / Received in final form 25 March 2010

Published online 19 May 2010 – © EDP Sciences, Società Italiana di Fisica, Springer-Verlag 2010

**Abstract.** Photoinduced structural phase transition (PSPT)s are reviewed in connection with recent experimental results. There are two key concepts: the hidden multi-stability of the ground state, and the proliferations of optically excited states. Taking the ionic (I)-neutral (N) phase transition in an organic charge-transfer (CT) crystal TTF-CA, as an example, we, briefly look back the essence of its PSPT, in terms of the CT exciton and the N-domain proliferation. Next, we are concerned with the discovery of a new photoinduced phase with inter-layer  $\sigma$ -bonds in a graphite. We will see the mechanism of this nonequilibrium phase transition, in terms of the proliferation of photo-generated inter-layer CT excitations in the visible region. At the Franck-Condon state, the resultant electron-hole pair is quite unstable, being easily dissipated into the two-dimensional electronic continuum, as plus and minus free carriers. However, by a small probability, the electron and the hole are bound as an inter-layer CT exciton. This exciton self-localizes, contracting the inter-layer distance and buckling the six membered ring of graphite, only around it. Thus a tiny  $sp^3$  nano-domain appears.

## 1 Introduction, equilibrium phases, non-equilibrium phases and photo-induced phase transitions

Large varieties of materials are now around us. These materials are such ones, that few kinds of macroscopic numbers of atoms or molecules are condensed with a definite composition ratio. While, without changing this chemical composition, a material can take various phases from gaseous and liquid phases to crystalline ones, as temperature decreases from high to low. Even at low temperatures, a material can take various crystalline phases, whose lattice structure and electronic state change as temperature decreases. However, all these states are so-called equilibrium phases, in the sense that the free energy of each state takes its global minimum at each temperature.

Let us now proceed to non-equilibrium phases generated from an equilibrium one by some external excitations or stimulations. Usually, these states are transient ones having higher energies than the equilibrium one, but, depending on the way of the stimulations or excitations, we can get much more varieties of states, even if the starting equilibrium phase is same. They also surely relax down to the starting equilibrium one after a period of time. However, if they are locally stable state, in the sense that their free energies take local minima separated from the global one by substantial energy barriers, the time required for the relaxation will be long. In that case, we can complete

necessary observations to determine their characteristics within this period of time. Hence, such a long-lived locally stable non-equilibrium phase is effectively same as the equilibrium ones.

Various amorphous crystals are well known as typical examples for these non-equilibrium phases [1]. They are brought about after being cooled down rapidly from their high temperature phases. The lifetime of the relaxation is believed to be much longer than the time scale of our daily life. Unfortunately, however, these amorphous crystals have no well-defined long range periodic crystalline or electronic order, since they are just amorphous.

Very recently, on the other hand, there discovered a new class of insulating solids, which, being shone by only a few visible photons, become pregnant with a macroscopic excited domain that has new structural and electronic orders quite different from the starting ground state (equilibrium phase). This phenomenon is called “photo-induced phase transition” and we can generate new long lived locally stable macroscopic non-equilibrium phases through the excitations or stimulations by a few visible photons. The purpose of this paper is to review recent studies on these phenomena.

## 2 Relaxation of optical excitations, hidden multi-stability

As is already well known, an electron in an insulating crystal induces a local lattice distortion around itself, when it

<sup>a</sup> e-mail: knasu@post.kek.jp

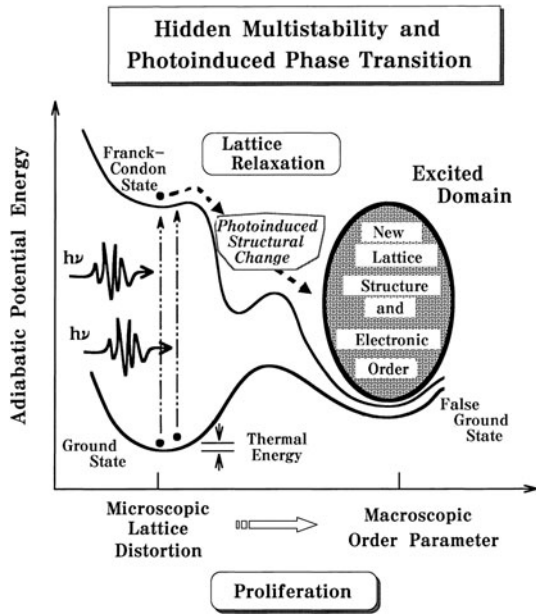


**Fig. 1.** Schematic and conceptual nature of photo-induced structural phase transition, hidden multi-stability and proliferation.

is excited by a photon. A sudden change of charge distribution appeared through this optical excitation, induces a motion of the crystal lattice surrounding the excited electron, so that the whole electron-lattice system will reach a new equilibrium position within the excited state. This phenomenon is called “lattice relaxation” of an optical excitation, and the resultant state is often called “photo-induced structural change”, as schematically shown in Figure 1. This relaxation phenomenon has been studied in detail, in various kinds of insulating crystals for these fifty years. According to the original concept of this lattice relaxation, however, it is tacitly assumed to be a microscopic phenomenon, in which only few atoms and electrons are involved [2].

In the recent years, on the other hand, there have been discovered many unconventionally photoactive solids, where the relaxation of optical excited states results in various collective motions involving a large number of atoms and electrons. In some cases, it results in a macroscopic excited domain with new structural and electronic orders quite different from the original ones. This situation can be called “photo-induced structural phase transition (PSPT)” [3–6].

These problems are closely related with the hidden multi-stability intrinsic to each solid. If the ground state of a solid is pseudo-degenerate, being composed of true and false ground states with each structural and electronic orders different from others, we call it multi-stable. In this case, the photo-absorption, being initially a single-electron excitation from the true ground state, can trigger local but macroscopic instabilities. The photo-absorption can induce low-lying collective excitations during the lattice relaxation, and can finally produce a false ground state at the expense to create boundaries between the two states.

Thus a local but macroscopic excited domain appears. In other words, the initially created single-electron excitation proliferates during the relaxation, and grows up to be a macroscopic order, as schematically shown in Figure 1.

The origin of the pseudo-degeneracy can be understood from the conceptional point of view, related with the cohesive mechanism of each solid. As mentioned before, the solid is composed of macroscopic numbers of few kinds of atoms or molecules with a definite composition ratio. However, even if the constituent atoms (molecules) are defined, the structural and electronic orders, which will be realized in the macroscopic ground state, are not always determined straightforwardly. For example, even in the case of alkali halide, the ionic state and the covalent one are two well-known candidates for the ground state [7]. Moreover, if there are two predominant but mutually conflicting elements in the original Hamiltonian, there appear two candidates that inherit this conflict. Thus, it is not extraordinary, but quite ubiquitous that we have the multi-stability or the pseudo-degeneracy with the true and false ground states.

It is also very important to see the relation between photo-induced phase transitions and the ordinary ones due to the thermal excitation. When the false ground state is so fortunate to be just above the true one, being easily excited by the thermal energy, we may get the ordinary phase transition, and can recognize the presence of this false ground state. However, there will be various other cases that the energy of the false ground state is too high to be excited thermally. Ordinary thermodynamic measurements can be concerned only with the true ground state or small excitations therefrom, and hence, they can never detect such hidden states. Even in these difficult cases, we can create the false ground state by the photo-excitation and the lattice relaxation therefrom, as schematically shown in Figure 1.

Such a false ground state always disappears finally within a finite life-time, and can never be permanent, as mentioned before. However, according to the recent progress of our laser spectroscopy techniques, an infinite life time is no more necessary for each state to be recognized as a well-defined state, provided that can last long enough to be clearly observed by other photons to detect it. At present, the time required for this type observation is usually less than a pico-second, and in some case, even a femto-second is enough.

Incidentally, let us briefly see, the difference between the present photo-induced phase transition and the so-called “new material design (or search)”, which is the most contemporary trend in the field of the material science. The one of most standard techniques for the new material design (or search) is to apply static external fields such as electric, magnetic fields, and (or) pressures onto a material, which is expected to give novel or anomalous properties, absent in other materials existing already. The other most standard technique is to design or synthesize the material by changing its chemical composition, little by little, so that it will show quite new properties.

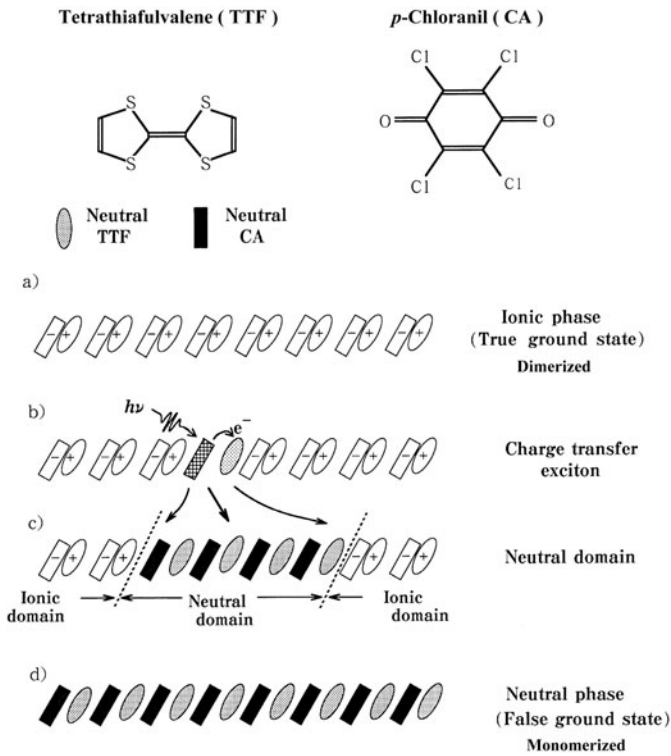


**Fig. 2.** Schematic nature of photo-induced ionic  $\rightarrow$  neutral structural phase transition in TTF-CA crystal. (a) Ionic phase, (b) Charge transfer exciton, (c) Neutral domain, (d) Neutral phase.

In the case of static external field, however, it changes all the electronic state of the material, both ground and excited states, unselectively. While photons have definite momentum, phase, helicity and energy. Hence, they can create only particular excited states, selectively and quite intensively. In contrast to the chemical design or synthesis, the photo-induced phase transition does not change the chemical composition of the material, but can realize new states. Thus the research for photo-induced phase transitions will be able to open a new multistoried concept for materials.

### 3 Photo-induced ionic-neutral phase transition in organic molecular crystal TTF-CA

As one of the typical examples for the PSPT, here, we will be concerned with the photo-induced ionic (I) $\rightarrow$  neutral (N) transition in an organic molecular crystal Tetrathiafulvalene-*p*-Chloranil, and review the present stage for its experimental studies. Both Tetrathiafulvalene (TTF) and *p*-Chloranil (CA) are planar organic molecules as schematically shown at the top of Figure 2, and their crystal has a quasi one dimensional (1-d) chain like structure, in which these two molecules are alternately stacked along this 1-d chain axis.

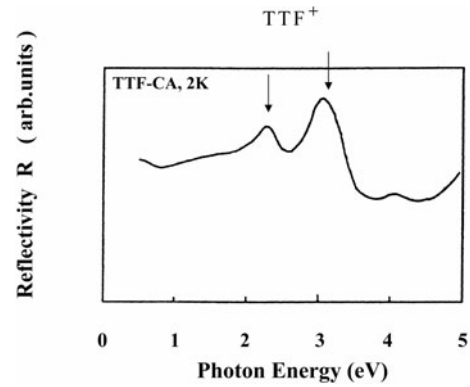


**Fig. 3.** Spectral shape of the original optical reflectivity ( $\equiv R$ ) of the TTF-CA crystal in the I-phase at 2 K. The exciting light is polarized perpendicular to the 1-d chain axis. Peaks at around 2.2 eV and 3 eV correspond to intra-molecular electronic excitations of TTF<sup>+</sup>. From reference [8].

In the true ground state of this crystal at absolute zero of temperature, both TTF and CA become a cation and an anion, respectively, and make a dimer with each other as shown in Figure 2a. This is called the I-phase. On the other hand, we also have the N-phase, in which neutral TTF and CA are stacked alternately without dimerization, as shown in Figure 2d. This is the accidentally pseudo-degenerate false ground state, and at absolute zero of temperature, it is just above the ionic true ground state.

Keeping this material in the low enough temperature, but shining a strong laser light of about 0.6 eV $\sim$ 2.3 eV on to it, we can generate the N-domain even in the ionic true ground state, as schematically shown in Figure 2c. This change was experimentally confirmed by the change of the optical reflectivity. The Figure 3 shows the spectral shape of original optical reflectivity of the TTF-CA crystal in the I-phase at 2 K, where the exciting light is polarized perpendicular to the 1-d chain axis [8]. In this spectrum, we can see characteristic peak structures at around 2.2 eV and 3 eV. These peaks correspond to intra-molecular electronic excitations of TTF<sup>+</sup>. Hence their intensities can be used as macroscopic indicators for the presence of cationic TTF molecules in this crystal.

In fact, when this crystal is shone by a light with an energy of 2.3 eV, we can get a relative change of this reflectivity, as shown in Figure 4 [9,10]. The intensity of the aforementioned peak at 3 eV is clearly seen to decrease. It means, not microscopic, but a macroscopic number of neutral TTF molecules (N-domains) have been generated in the I-phase. This is nothing else but the PSPT. From this decrease of the peak intensity, Koshihara has determined that the domain is composed of about 200 $\sim$ 1000 neutral pairs, and it can last for about  $10^{-3}$  s [9].

#### 3.1 Threshold excitation intensity and initial condition sensitivity

For this transition, we can think of the following simple and intuitive scenario as schematically shown from

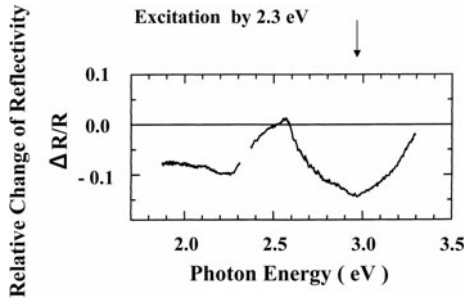


**Fig. 4.** Relative change ( $\equiv \Delta R/R$ ) of the reflectivity, when the TTF-CA crystal is shone by a light with an energy of 2.3 eV. From reference [9,10].

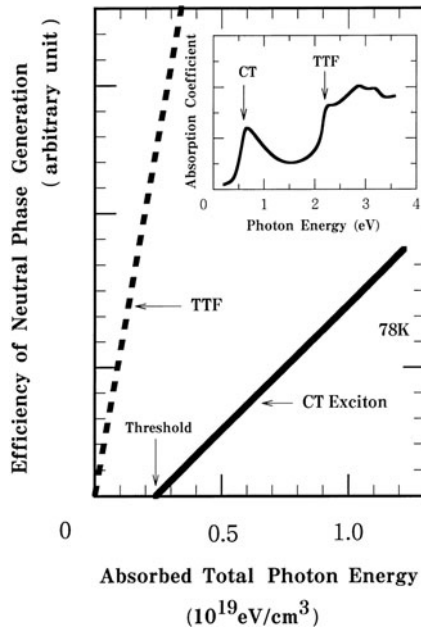


**Fig. 5.** Efficiency of neutral phase generation in TTF-CA as functions of total absorbed photon energy. The horizontal axis denotes the total photon energy absorbed in the unit volume of the TTF-CA crystal. This total energy is calculated by taking the three quantities into account: the absorption coefficient, the energy of the photon, and its intensity. The thick solid line is the CT excitation (0.6 eV), while the thick dashed line is the intra-molecular excitation (2.3 eV). The small inset denotes the light absorption spectrum of the TTF-CA crystal. From reference [10].

Figure 2b to Figure 2c. That is, a single photon can make a single charge transfer (CT) excitation between neighboring molecules, which is just equal to a neutral pair generation. After that, the number of this neutral pair will increase like a domino game. However, by the recent experimental studies shown in Figure 5 [10], this simple scenario is proved wrong.

In this Figure, we have shown the photo-absorption spectrum of TTF-CA, as a small inset. It has two peaks at 0.6 eV and also at 2.2 eV. The first one, being the elementary optical excitation of this crystal, corresponds to the aforementioned inter-molecular CT excitation. Among a macroscopic number of neighboring ion pairs ( $\text{TTF}^+$

and  $\text{CA}^-$ ) in Figure 2a, only a single neighboring ion pair returns back to a neutral pair (TTF and CA) by this excitation as shown in Figure 2b, and this neutral pair also itinerates along the crystal axis, keeping all other pairs still ionic. This is nothing else but the so-called inter-molecular CT exciton, wherein a hole and an electron (a positive charge and a negative one relative to the I-phase) are bound together, so that they are always at neighboring two molecules with each other, even if their center of mass itinerates. While, the second peak at 2.2 eV corresponds to an intra-molecular electronic transition of TTF, just like the case of the aforementioned 3 eV peak. The thick solid line in Figure 5 denotes the efficiency of the N-phase generation as a function of the exciting photon intensity, when the photon energy is fixed at this CT exciton (0.6 eV). We can clearly see that there is a threshold in the intensity, below which the macroscopic N-phase can never be generated. It means that a single CT exciton alone can never result in the macroscopic N-phase, but only through a nonlinear cooperation between several photo-excited CT excitons, the new phase can be attained. The presence of this threshold is the first note-worthy characteristic of the TTF-CA crystal.

The second note-worthy characteristic, which we can see from Figure 5, is the difference between the dashed line and the aforementioned thick solid line. Exactly speaking, the horizontal axis of this figure does not simply denote the photon intensity itself, but denotes the total photon energy, which is absorbed in the unit volume of the TTF-CA crystal. This total energy is calculated by taking the three quantities into account; the absorption coefficient, the energy of the photon, and its intensity. Thus, we can compare the 0.6 eV excitation and the 2.2 eV excitation (the thick dashed line) on an equal footing. For example, if we focus on the point with a value 0.25 of the horizontal axis in Figure 5, we can find that the efficiency becomes very high or almost zero, depending sensitively on the photon energy, although the total absorbed photonic energies are same each other. Not only these two cases, we can also excite using various other photons in between (0.6 eV~2.2 eV), keeping the total absorbed photonic energies are same. However all these excitations give the efficiencies different with each other, and ranging between the two lines in Figure 5.

From this fact, we can immediately conclude that it is not the ordinary thermal phase transition. In the experimental studies for photo-induced phase transitions, the first thing we have to examine is, whether it is the ordinary thermal phase transition or not. Because, the absorbed photons may often be converted into heat in the crystal, raising up its temperature, and may indirectly result in the ordinary thermal phase transitions. In the case of this indirect thermal phase transition, however, its generation efficiency will depend only on the total absorbed photon energy, and will never sensitively depend on the way or type of the excitation. While, Figure 5 shows that the generation efficiency quite sensitively depends on the type of the excitation, that is, the exciting photon energy, even if the total absorbed photonic energies are same. If

we return back to Figure 1, the aforementioned two types of excitations start from the common ground state minimum equally, and moreover, the energies of the final states of the Franck-Condon transition are almost same.

Here, we should emphasize the so-called Franck-Condon principle. The optical transition can complete within a time of the order of femto-second, provided that its transition energy is in the visible region. While, the period of oscillation of a crystal lattice or phonon is of the order of pico-second. Thus, the configuration of the crystal lattice can never change during the optical transition, and hence, it can occur only vertically as schematically shown in Figure 1. Consequently, possible differences between the aforementioned two transitions are only in the electronic natures of these Franck-Condon type excited states, from which the lattice relaxation and the proliferation start. However, this small difference in the initial state of the relaxation, afterwards diverges and finally determines occurrence or nonoccurrence of the photo-induced phase transition. This is the so-called “initial condition sensitivity”, peculiar to the dynamics of nonlinear systems.

As is well known, the initial condition sensitivity has been studied mainly from the mathematical point of view, by taking classical nonlinear model systems with only a few degrees of freedoms [11]. The setting up the initial condition, in this case, is also purely mathematical and artificial procedure in order to solve nonlinear differential equations that describe these model systems. On the other hand, the present case is the formation of a macroscopic order in a real material, and the setting up the initial condition itself is also a real physical process. As mentioned before, it is set by choosing the spatio-temporal pattern of the exciting photon pulse, and hence, it is in compliance with the quantum uncertainty. Thus the studies for the photo-induced phase transitions open new aspects of the nonlinear dynamics and self-organization phenomena. Theoretical studies from this point of view, have already been undertaken by us [12,13].

### 3.2 Real time dynamics and coherent oscillation

The real time dynamics of this PSPT process was also experimentally clarified by Iwai [14], and also by Okamoto [15] in detail. They are shown by Figure 6, in connection with the temperature dependence of the threshold type behavior, or the criticality of the aforementioned proliferation. In this case, the reflectivity change  $-\Delta R/R$  at the second peak (2.25 eV) of Figure 3 was measured after the pulse excitation of the CT exciton peak (0.65 eV) shown in the inset of Figure 5. The intensity of this excitation is  $2 \times 10^{14}$  photons/cm<sup>2</sup> independently of temperature, and it corresponds to rather weak excitation. We can see that the starting rises of the reflectivity change, (the total numbers of the N-pairs initially created), are almost same in both two cases with 4 K and 77 K. However, the reflectivity change afterward gradually decreases in the case of 4 K, while it surely increases in the case of 77 K. Thus, the failure or the success of the proliferation depends on the temperature. The ordinary

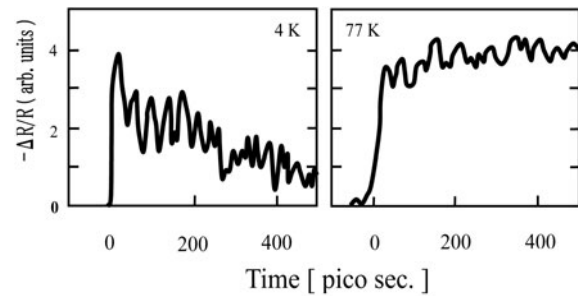


**Fig. 6.** The real time dynamics of the neutral phase generation and its temperature dependence. The reflectivity change  $-\Delta R/R$  at the second peak (2.25 eV) of Figure 3 was measured, after the pulse excitation of the CT exciton peak (0.65 eV), shown in the inset of Figure 5. The intensity of this excitation is  $2 \times 10^{14}$  photons/cm<sup>2</sup> independently of temperature. From reference [14].

thermodynamic phase transition from I to N in TTF-CA occurs at 84 K, and hence, the proliferation also becomes successful as temperature approaches to it.

We can also see that this reflectivity change oscillates with a period of about 40 pico-second as a function of time. It means that the initially created N-domain grows (or shrinks) not monotonically, but oscillatory. As already well-known in the gas phase chemical reactions or in the molecular collisions, the complicated reaction often proceeds not monotonically but oscillatory. It is due to the fact that the real geometrical path of the complicated chemical reaction often vibrates strongly but perpendicularly to the most probable classical path, whose energy is always the lowest at each step of this reaction process [16]. This is the so-called “bobsled” effect [17]. In the case of the present N-domain formation shown in Figure 2c, it is also a kind of complicated and collective chemical reaction that occurs in the multi-dimensional coordinate space of the crystal lattice of TTF-CA. Thus, such a coherent oscillation or the bobsled effect has been clearly shown to play an important role even in the present PSPT.

## 4 Material variety and new measurement methods

As seen above, the PSPT study has developed, using TTF-CA as a key material. However, this type study is now going on in various kinds of materials, not only in organic charge transfer crystals other than TTF-CA [18,19], but also, in spin cross over complexes [20,21], mixed valence transition metal complexes [22], Prussian blue analogues [23], Perovskite type or other inorganic metal oxides [24,25], and even in the ordinary conductive or metallic materials [26,27].

The objective phenomenon is also extended not only to the structural phase transitions, but also to the photo-induced spin state or magnetic transitions [28], to photo-induced dielectric ones [29,30], and even to the various insulator-metal transitions [31–33]. The recently published

proceedings [6] in this field of study cover most of them within a volume.

Meanwhile, the standard technique to observe or to measure these PSPT phenomena has been the so-called modulation spectroscopy, in which another visible photon is also shone to detect the aforementioned spectroscopic change between before and after the transition. Very recently, however, we have succeeded to observe the photo-induced structural phase transition more directly by using the time-resolved X-ray diffraction [34,35]. Using the TTF-CA crystal mentioned before, Collect [35] has succeeded to detect the PSPT from the N-phase to the I-phase at 93 K, by the time-resolved X-ray diffraction method.

Moreover, the scanning tunnelling microscope (STM) is also devised, in connection with the photo-induced structural phase transition from the graphite to the diamond [36], as well as the time resolved electron diffraction study for this phenomenon [37].

## 5 Brief review for theories

Lets us briefly review theoretical studies on the PSPT. As shown by Toyozawa [38], the PSPT phenomenon is closely related to the self-localization of an exciton in an insulating crystal. It can be simply described by the following model Hamiltonian ( $\equiv H_F$ ),  $\hbar = 1$ ,

$$H_F = -T_F \sum_{\ell, \ell'} [F_{\ell'}^+ F_{\ell} + h.c.] + \sum_{\ell} (E_g + 6T_F - \omega_0 S Q_{\ell}) \times F_{\ell}^+ F_{\ell} + \frac{\omega_0}{2} \sum_{\ell} Q_{\ell}^2. \quad (1)$$

Here,  $T_F (>0)$  is the resonant transfer (energy) of an exciton from a lattice site  $\ell$  to its nearest neighbouring sites  $\ell'$  in a simple cubic crystal, and  $F_{\ell}^+$  is the creation operator of this exciton at the lattice site  $\ell$ . It is not the CT exciton, but an intra-atomic (or intra-molecular) one in each lattice site. As schematically shown in Figure 7,  $E_g$  denotes the energy gap of this insulator, while  $S$  is the dimensionless coupling constant of this exciton to a site localized phonon, of which energy and dimensionless coordinate are  $\omega_0$  and  $Q_{\ell}$ , respectively. The kinetic energy of this phonon is neglected, because of the adiabatic approximation. In ordinary insulators,  $E_g$ ,  $6T_F$  and  $\omega_0 S$  are quantities of the order of eV, while  $\omega_0$  is 10 meV or so.

The eigen-state ( $\equiv |\Psi(Q_{\ell})\rangle$ ,  $\langle \Psi | \Psi \rangle = 1$ ) of this  $H_F$  will be given as a function of  $Q_{\ell}$  and unknown at present, but we determine it under the condition that the total number of the exciton is just one,  $\sum_{\ell} F_{\ell}^+ F_{\ell} = 1$ . After formally taking the average of  $H_F$  with respect to this unknown  $|\Psi\rangle$ , we can apply the Hellmann-Feynman theorem to equation (1), and can get as,

$$\frac{\partial \langle \Psi | H_F | \Psi \rangle}{\partial Q_{\ell}} = 0, \quad \langle \Psi | F_{\ell}^+ F_{\ell} | \Psi \rangle = \frac{Q_{\ell}}{S}. \quad (2)$$

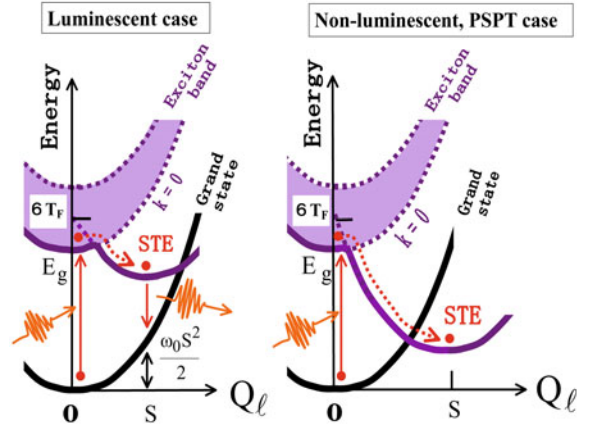


**Fig. 7.** Schematic nature of exciton self-localization and the start of the PSPT. The Luminescent case (left), and the non-luminescent, PSPT case (right). The self-localization formally starts from the exciton band center, whose energy is  $6T_F$  higher than the exciton band edge with the energy  $E_g$ .

Substituting this equation (2) into the original equation (1), we also get

$$\langle H_F \rangle = (E_g + 6T_F) - T_F \sum_{\ell, \ell'} [\langle F_{\ell}^+ F_{\ell'} \rangle + \langle F_{\ell'}^+ F_{\ell} \rangle] - \frac{\omega_0 S^2}{2} \sum_{\ell} \langle F_{\ell}^+ F_{\ell} \rangle^2, \quad (3)$$

where  $\Psi$  is omitted in the averages  $\langle \dots \rangle$ , for simplicity. We should note that this equation (3) holds only at local minimum (or extremum) points in the multi-dimensional coordinate space spanned by  $Q_{\ell}$ , since it is obtained by using equation (2).

When the exciton-phonon coupling is sufficiently strong,  $6T < (\omega_0 S^2)/2$ , according to Shinozuka [39], we have only two types of minima in the adiabatic potential energy surface of the excited state, as schematically shown in Figure 7. One is the globale minimum with  $\langle F_{\ell}^+ F_{\ell} \rangle = \delta_{\ell,0}$ , being localized, say, at the origin  $\ell = 0$  with a large lattice displacement,  $Q_0 = S$ . Its electronic energy ( $(E_g + 6T_F) - \omega_0 S^2$ ), given by the second term of equation (1), formally starts from the exciton band center ( $E_g + 6T_F$ ), but goes below the exciton band, as a local lattice displacement  $Q_0$  is self-induced, ( $0 \rightarrow S$ ). It is called self-trapped, (or self-localized) exciton (STE) state. The second local minimum is  $\langle F_{\ell}^+ F_{\ell} \rangle = 1/N$ , where  $N$  denotes the total number of the lattice sites in the crystal. This is the plane-wave state of the exciton whose wave-vector ( $\equiv k$ ) is zero,  $k = 0$ , and its energy is just the energy gap  $E_g$ . The final state of the Franck-Condon excitation by light is this plane wave state, being the lowest one within the exciton band. While, after the lattice relaxation, as schematically shown by the dashed allow in Figure 7, the whole system reach the STE state. We should also note that, at this largely displaced lattice configuration, even the elastic energy of the ground state, as well as that of the STE, increases upto  $\omega_0 S^2/2$ , since the lattice distortion, (the last term of Eq. (1)), is common to all states. If the

total energy of this STE state is above the ground state one at this lattice configuration,

$$(E_g + 6T_F) - \frac{\omega_0 S^2}{2} > \frac{\omega_0 S^2}{2}, \quad (4)$$

this STE state finally disappears with a luminescence, of which energy is a little smaller than the exciting one, as shown in the left part of Figure 7. This is the ordinary situation widely realized in the luminescent insulator.

As shown in the right part of Figure 7, however, if the exciton-phonon coupling is so large as to relax down even lower than the ground state at this largely displaced lattice configuration,

$$0 < (E_g + 6T_F) - \frac{\omega_0 S^2}{2} < \frac{\omega_0 S^2}{2}, \quad (5)$$

the system becomes non-luminescent, and the STE remains forever within the adiabatic approximation at absolute zero temperature. This is nothing but the start of the PSPT.

Of course, in the aforementioned picture, the energy of the STE is tacitly assumed to be always positive. However, as this energy close to zero, we have to proceed from the one exciton picture to a collective many-exciton picture as shown in Figure 1. Using the 1-d localized ( $T_F = 0$ ) many-exciton model, Hanamura and Nagaosa [40] have already studied the condition of the PSPT, wherein the aforementioned collectivity is quite simply but symbolically taken into account through the bi-linear coupling between  $Q_\ell$  and  $Q_{\ell'}$  ( $\ell \neq \ell'$ ). In connection with the photopolymerization problem of the diacetylene, they concluded that the PSPT occurs when  $\omega_0 S^2$  is only a little less than  $E_g$  and also this bilinear coupling is sufficiently strong. The real time dynamics by this 1-d localized model was afterward extended within the adiabatic approximation by Koshino and Ogawa [41], under the light of the domino effects in the PSPT. While, for the 2-d system, Ishida [42] has extended this localized model including the diabatic (nonadiabatic) effects of phonons, and has clarified the initial condition sensitivity and the fractal pattern formation dynamics of the PSPT.

In the case of the itinerant many-electron model, we have to take into account the inter-electron Coulomb repulsion and the electron phonon coupling more directly, and various approximations are devised for the PSPT problem. The Hartree-Fock method for long range inter-electron interactions and the adiabatic approximation for electron-phonon couplings are devised to clarify the electronic and lattice structures of the TTF-CA by Sakano [43], and also by Huai [44]. Moreover, the following various methods are also devised to overcome difficulties in the real time dynamics of quantum many-body systems, that is, the exact diagonalization method for small clusters [45], the density matrix renormalization group method [46,47], and the dynamical mean field theory [48]. Most of these theoretical works are systematically reviewed by Yomemitsu [5].

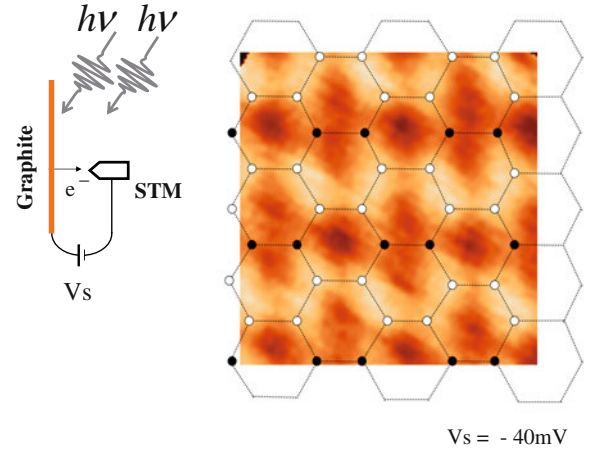


**Fig. 8.** The scanning tunneling microscope (STM) image of the first layer of the graphite after being irradiated by visible photons at the room temperature. The dotted lines, white and black circles are only for eye guide.  $V_s$  is the sample voltage. From reference [36].

## 6 New photo-induced phase in graphite crystal

Let us now proceed to the nano-scale  $sp^2 \rightarrow sp^3$  collective conversion in a graphite crystal by a visible light irradiation. The hexagonal graphite crystal is a layered material made only of carbon atoms with the completely planar  $sp^2$  bonds among them. Each graphite layer has a two-dimensional semi-metallic continuum electronic state, with only a weak inter-layer interaction. Using such a ubiquitous graphite crystal, very recently, Kanazaki has discovered a new PSPT, whose resultant scanning tunneling microscope (STM) image is shown in Figure 8 [36]. The dotted lines, white and black circles in this figure are only for eye guide, and  $V_s$  is the sample voltage. We can see that the six membered ring in the first layer of the crystal, being originally completely planar, buckles after the visible light irradiation in such a way that 4 carbons rise up, while the residual 2 sink down and close to the second layer, forming new inter-layer  $\sigma$  ( $sp^3$ ) bonds.

We here summarize the essential points of this experiment. (1) The exciting laser light with the energy of about 1.6 eV, should be polarized perpendicular to the graphite layers, while the light polarized parallel to the layer gives no change. It means only the inter-layer CT excitations can trigger this phase transition. (2) This phase transition is a nonlinear multi-photon process, but less than the 10-photon one. (3) The exciting light should be a femto-second pulse, while a pico-second one gives almost no contribution. It means, only a transient generation of an excited electronic wave-packet in the semi-metallic continuum, can efficiently trigger the phase transition, while a monochromatic or stationary electronic excitation is not effective. (4) The resultant nano-scale domain of new phase includes 1000 carbons or so. The STM image shown in Figure 8 suggests us that a novel and periodic inter-layer  $\sigma$  ( $sp^3$ ) bond is established in this non-equilibrium

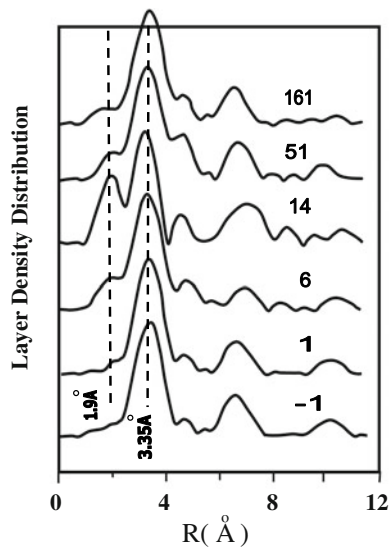


**Fig. 9.** The inter-layer density distribution as a function of the distance  $R(\text{Å})$ . The elapsed time after the laser pulse excitation is written in the upper right hand side of each distribution function by the unit of pico-second. From reference [37].

phase, and this new structure is stable for 10 days or so, at room temperatures.

Independently of this STM study for the graphite crystal, the time resolved electron diffraction study for this phenomenon is also undertaken as shown in Figure 9 [37]. In this case, the excitation is a femto-second laser pulse with the energy of 1.55 eV, and its intensity is 77 mJ/cm<sup>2</sup>, being rather strong, but it is surely below the damaging threshold of this crystal. The inter-layer density distribution was measured as a function of the distance  $R(\text{Å})$ , by the time resolved electron diffraction method, using the electron beam with an energy of 30 KeV. The elapsed time after this pulse excitation is written in the upper right hand side of each distribution function by the unit of pico-second. We can clearly see that, about 14 pico-second after the pulse excitation, a new inter-layer structure appears at  $R = 1.9 \text{ Å}$ , as well as the original inter-layer one at  $R = 3.35 \text{ Å}$ .

One can easily infer, that this phenomenon is closely related with the so-called graphite-diamond ( $sp^2 \rightarrow sp^3$ ) conversion, which has a very long history of considerable experimental and theoretical researches. This conventional graphite-diamond structural phase transition, being the first-order one in the thermal equilibrium, is already well known to occur, only under the very high pressure (15 GPa) and the very high temperature (3000 K) [49], or under irradiations of strong electron or X-ray beams [50,51], whose energies are of the order of magnitude greater than that of visible photons. In these conventional syntheses of the diamond from the graphite, a large amount of macroscopic energy is usually given to all over the crystal, and the global structural conversion occurs at almost all parts of the crystal, simultaneously.

Thus, the conventional graphite  $\rightarrow$  diamond conversion is quite different, from the present photoinduced

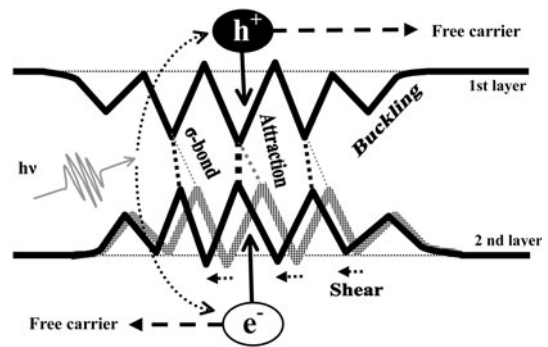


**Fig. 10.** The schematic nature of the photo-generated electron-hole pair, its free carrier type dissipation, its self-localization, the buckling, the shear displacement, and the inter-layer  $\sigma$  bonds.

phase transition. In the latter case, only a microscopic energy of few photons, enough to nucleate a minimum kernel of the new phase, is given to a local and limited area of the crystal. This minimum kernel will proliferate stepwise, according to the hidden instability (or the multi-stability) intrinsic to the graphite crystal. In fact, at low temperatures and the atmospheric pressure, the graphite is the true ground state of macroscopically condensed carbon atoms, while the diamond is the false ground state only about 0.02 eV (per carbon) higher than the graphite [52], and the adiabatic energy barrier between them is only about 0.3 eV per carbon [53–55]. Thus, the hidden multi-stability is well prepared in this system, just described in Figure 1.

## 6.1 Possible scenario

Let us see a possible scenario to describe the aforementioned photoinduced phase transition. One can easily infer, that the whole process to photoinduce the new domain in the graphite crystal will be a very complicated one. Hence, in the present colloquium paper, we will see only the early stage of this complicated phenomenon. It will be triggered by the aforementioned lattice relaxation and the proliferation of photo-generated inter-layer CT excitations. This excitation is in the visible region, and at the Franck-Condon state, the resultant electron-hole pair, spanning neighboring two layers, is quite unstable, being easily dissipated into the 2-d semimetallic continuum electronic states, as plus and minus free carriers. In fact, the graphite has been well-known as a good electric conductor.

As schematically shown in Figure 10, however, by a small but finite probability, the electron and the hole will become stable, as the lattice relaxation proceeds, being bound with each other, just like an exciton, through the inter-layer Coulomb attraction. This exciton-like state self-localizes, by contracting the inter-layer distance and buckling the six membered ring of graphite, only around it. Thus, local inter-layer  $\sigma$  bonds are expected to be formed, or a tiny  $sp^3$  nano-domain will appear in the semi-metallic continuum.

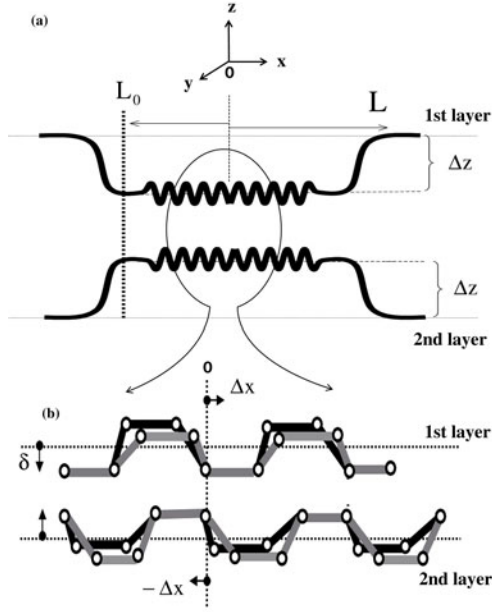


**Fig. 11.** The schematic natures of (a) the disk type displacement, and (b) the buckling of the six membered ring.  $L$ ,  $L_0$ ,  $\Delta z$ ,  $\Delta x$  and  $\delta$  are variational parameters.

One can easily infer, that the straightforward contraction of the inter-layer distance in the hexagonal graphite with the  $ABAB\dots$  stacking, may cause a mismatch of the inter-layer  $\sigma(sp^3)$  bonds. Hence, as schematically shown in Figure 10, a local shear type displacement will also occur between two layers, so as to self-adjust this mismatch. It was suggested by the experiments of Shirotni [56].

We should note that these successive deformation processes are nothing but the quantum and spontaneous broken symmetries, triggered only by the visible light irradiation and the subsequent self-localization.

## 6.2 Energetics and adiabatic barrier

Let us, at first, see the increase of the total adiabatic energy due to the aforementioned nano-scale  $sp^3$  domain formation, relative to the ground state of the hexagonal graphite crystal. We start from the complete graphite structure with the intra-layer bond length 1.42 Å and the interlayer bond length 3.35 Å. The local deformation of the lattice starting from this complete graphite is introduced by the following trial displacement pattern

$$z = \begin{cases} \bar{z} - \Delta z, & (\sqrt{x^2 + y^2} \leq L_0) \\ \bar{z} - \Delta z \frac{\tanh[\theta(\sqrt{x^2 + y^2} - L)] - 1}{\tanh[\theta(L_0 - L)] - 1}, & (\sqrt{x^2 + y^2} > L_0) \end{cases}, \quad (6)$$

and it is also shown in Figure 11 schematically. In equation (6) and Figure 11a,  $x$ ,  $y$  and  $z$  denote the Cartesian coordinates of the carbon atom, and  $\bar{z}$  is the  $z$  coordinate of the original graphite. This disk type intrusion from the

graphite is assumed to be perpendicular to the graphite layers.

The center of the mass of the whole system will be unchanged. Hence the deformation in the second layer is just the inverse of the first one with respect to the  $x$ - $y$  plane, which is at the center of Figure 11a. Meanwhile, the buckling shown in Figure 11b with the amplitude  $\delta$  ( $\geq 0$ ) is a such one that two thirds of carbons rise up, while one third of carbons sinks down in each six membered ring, keeping the center of mass of the ring unchanged. The local shear displacement shown in Figure 11b with amplitude  $\Delta x$  ( $\geq 0$ ) is a such one that each layer shifts oppositely to improve the bonding mismatch between the layers. The spatial patterns of the buckling and the shear are also assumed to be same as that of the intrusion  $\Delta z$  shown in equation (6). These parameters  $\Delta z$ ,  $\theta$ ,  $L_0$ ,  $L$ ,  $\delta$  and  $\Delta x$  in equation (6) and Figure 11 are variational ones that characterize the domain pattern, and should be determined under the condition that they as a set, not globally, but only locally minimize the total energy. For later convenience, we define the domain size as the region that the carbons sunk down more than  $\Delta z/2$ , and the total number of carbons in it, is referred to  $N_d$  hereafter.

To calculate the total energy increase due to this nano-domain immersed in the graphite crystal, we can use the semi-empirical potential theory [52]. The total carbons in this nano-domain are expected to be about 1000. Moreover, to correctly calculate the energy increase at around the domain boundary, we have to prepare at least 10 000 carbons per layer as the surrounding original graphite. To handle such a very large number of carbons ( $N \approx 20\,000$ ), the local density functional (LDF) theory is not so convenient. Hence, as a first trial, Ohnishi [57] has calculated using the semi-empirical Brenner potential theory.

The total energy ( $\equiv E_{tot}$ ) by this method is given as

$$E_{tot} = \sum_{i,j(<i)} \{V_R(r_{ij}) - B_{ij}V_A(r_{ij})\} f(r_{ij}), \quad (7)$$

where  $V_R$  and  $V_A$  are repulsive and attractive radial two-body pair potentials similar to the Lenard-Jones ones. While the bond order function  $B_{ij}$  takes into account the three- or four-body force as a function of the bond angle between neighbouring carbons, and  $f(r_{ij})$  is the cut-off function of the force range with the bond length  $r_{ij}$  between  $i$ th and  $j$ th carbons. In contrast to the widely used Lenard-Jones typed two-body potential theory, the Brenner theory thus takes the many-body effects more than the two-body between neutral carbons into account. We can adopt the Brenner potential I, which reproduces almost all existing experimental and theoretical data of various carbon clusters. It successfully describes vacancies, interstitials and dislocations in large carbon clusters. In fact, this parameterization (Brenner I) well reproduces the binding energy of the graphite and the diamond. We can check, under the uniform transformation condition, the value of the adiabatic energy barrier between the graphite and the diamond. It is 0.35 eV/atom, agrees well with the aforementioned LDA results [53–55].



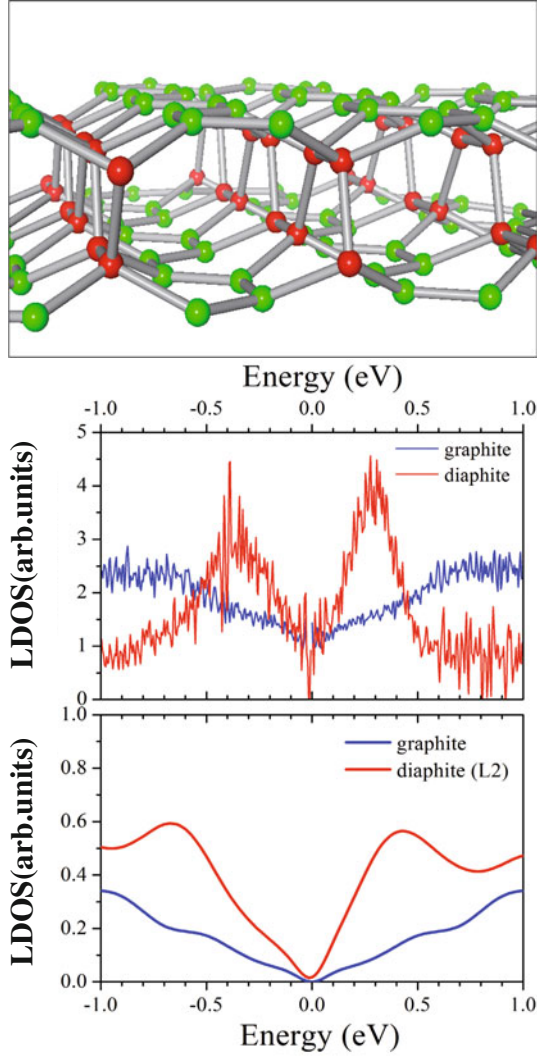


**Fig. 13.** (a) The calculated structure of the L2 diaphite domain. The red carbons are forming the interlayer  $\sigma$  bonds by sinking down from the original layer, while the green ones are forming the surface by rising up from the original. (b) The upper half is the LDOS determined by the aforementioned STM method [36] experimentally. The lower half shows the calculated LDOS of the red carbon at around the center of the L2 diaphite domain. From reference [57].

( $\equiv \Delta e_{ps}$ ) between them, and the four basic hopping integrals ( $\equiv V_{ss}, V_{sp\sigma}, V_{pp\sigma}$  and  $V_{pp\pi}$ ) among them, are taken into account only up to nearest neighbors. Their values at the bond length  $r_0 = 1.54 \text{ \AA}$ , are taken as,

$$\begin{aligned} \Delta e_{ps} &= 8.346 \text{ eV}, V_{ss} = -4.14 \text{ eV}, V_{sp\sigma} = 5.689 \text{ eV}, \\ V_{pp\sigma} &= 7.758 \text{ eV}, V_{pp\pi} = -2.489 \text{ eV}, \end{aligned} \quad (8)$$

so that they as a set reproduce the LDF result. While, they are also scaled according to the Harrison's rule [61], that is, all these hopping integral  $Vs$  at the other bond length ( $\equiv r$  ( $\text{\AA}$ )) are given as

$$V(r) = V \left( \frac{r_0}{r} \right)^2. \quad (9)$$

Using this tight-binding approximation, we can calculate the LDOS at each carbon atom. In the L2 diaphite domain, as shown in Figure 13a, however, we have two types of carbons, distinguished by the red and the green colors. The red carbons are forming the interlayer  $\sigma$  bonds by sinking down from the original layer, while the green ones are forming the surface by rising up from the original. The lower half of Figure 13b shows the LDOS of the red carbon at around the center of the L2 diaphite domain. We can clearly see that gap states appear at about  $\pm 0.5 \text{ eV}$  around the Fermi level, which is at the origin on the horizontal axis of Figure 13b. While, we can also see that the semi-metallic nature of the original graphite is still well kept. That is, the diaphite domains, are immersed in the semi-metallic state, resulting in a pseudo gap structure around the Fermi level. The upper half of Figure 13b is the LDOS determined by the aforementioned STM experimentally. These two results agree quite well with each other.

#### 6.4 Early stage dynamics and self-localization

As shown in Figure 10 and Section 6.1, the irradiation of visible lights polarized perpendicular to the graphite layer causes the inter-layer CT excitation, resulting in an electron-hole pair spanning neighboring two layers. The wave length of visible light is quite longer than the lattice constant of the graphite. This means that the wave vector of the visible photon is almost zero, because it is extremely smaller than the wave vectors of an electron, a hole and phonons in the first Brillouin zone. Consequently, the initial excited state is the Bloch wave whose total wave vector is almost zero, having the same translational symmetry as that of the crystal. In other words, the electron-hole pair excitation occurs coherently, at any places in the graphite layer with no quantum phase difference among them, under the condition that the total number of this excitation is equal to one.

On the other hand, as also shown in Section 6.1 and Figure 10, this electron-hole pair in the Franck-Condon state, is quite unstable. It will be easily dissipated into the two-dimensional (2-d) semi-metallic continuum electronic state as plus and minus free carriers, because of the good conductivity of the graphite. However, by a small but finite probability, the electron-hole pair is expected to become stable as the lattice relaxation proceeds, being bound with each other just like an exciton, through the inter-layer Coulomb attraction. This exciton-like state will self-localize at a certain point of the layer, by contracting the inter-layer distance only around it. After the large contraction of the inter-layer distance, the quantum coherency between the self-localized exciton states is lost, even if the excitations are at the neighboring lattice sites. This relaxation with the lattice distortion from the Bloch wave to the self-localized state can occur spontaneously anywhere of the lattice with the same probability. It is only due to the quantum fluctuations, and can occur even at absolute zero temperature. As a result,

the translational symmetry of the exciton state is broken. Thus, by locally contracting the inter-layer distance, a tiny insulating domain appears as shown in Section 6.2 and Figure 12. Through further pulse excitations by several visible photons, a lot of  $\sigma$ -bonds are formed stepwise, and the diaphite domain with a pseudo gap appears in the graphite layer as shown in Section 6.3 and Figure 13.

Thus, one of the most important points of the present PSPT is to know how large the probability of the self-localization is, relative to the free carrier type relaxation. For this reason, one should calculate the early-time non-adiabatic dynamics of an electron-hole pair, which is almost instantaneously excited by a femto-second photon pulse. In this case, we can focus only in the vicinity of the Franck-Condon state, and have to determine the branching ratio between these two relaxation channels, that is, the free carrier type relaxation versus the self-localization.

Our process starts from the electron-hole pair excited by the visible photon, spanning neighboring two layers. Before this excitation, the graphite layers have a 2-d semi-metallic continuum electronic state, with only a weak inter-layer interaction. Therefore, we can consider a minimal model with only a pair of distant layers, consisting of an electron, a hole, and also local phonons whose mode contracts the inter-layer distance. As undertaken by Radosinski [62] for the first time, the model Hamiltonian ( $\equiv H, \hbar = 1$ ) for this problem, can be taken as

$$H = H_{e-h} + H_p + H_c. \quad (10)$$

The first term  $H_{e-h}$  denotes the transfer energy of an electron and a hole given as

$$H_{e-h} = \sum_{i=1,2} \sum_{j=1,2} \sum_{\ell,\ell'} T(\ell - \ell') a_{\ell ij}^+ a_{\ell' ij}, \quad (11)$$

where  $a_{\ell ij}^+$  is the creation operator of an electron ( $i = 1$ ) or a hole ( $i = 2$ ) at the  $\ell$  th site of the  $j(=1, 2)$ th layer. For simplicity, the spin is neglected.  $T(\ell)$  is the inter-site transfer energy and given through the Fourier transformation of the dispersion relation ( $\equiv E(k)$ ),

$$T(\ell) = N^{-1} \sum_k E(k) e^{-ik\ell}, \quad (12)$$

where  $N$  is the total number of the lattice sites in a layer.

Around the Fermi level of a graphite layer, there are several energy bands coming from the hybridization between the  $2s$  and  $2p_\pi$  orbitals of carbon atoms. They are almost symmetric with respect to the Fermi level, and extend in a wide energy region from about  $-20$  eV to  $20$  eV [63,64]. In the present review paper, however, we are interested only in the visible excitations with the energy  $\pm 4$  eV around the Fermi level, and this region is mainly related with  $2p_\pi$  orbitals of carbons. Hence, we can assume this energy dispersion  $E(k)$  to be a  $V$ -shape (the Dirac cone), given as

$$E(k) = \sqrt{k_x^2 + k_y^2}, \quad |k_x| \leq \pi, |k_y| \leq \pi, \quad (13)$$

wherein  $k_x$  and  $k_y$  are the Cartesian components of the wave vector  $k$ , and the lattice structure of the layer is

also assumed to be the 2-d square lattice, only for simplicity. The electronic state on which this Hamiltonian is mainly based, is the  $2p_\pi$  orbital of carbons. This situation is quite simple, but well describes the semi-metallicity of the graphite layer around the Fermi level. The Fermi point of this model is at the  $\Gamma$  point of the Brillouin zone, while that of the real graphite is at the  $K$  point. However, this difference will give no serious effect for our final result, since the Fermi point can be moved to other points by an appropriate gauge transformation.

The second term  $H_p$  of equation (10) denotes a localized phonon with an energy ( $\equiv \omega$ ) at the  $\ell$ th site, and given as

$$H_p = \frac{\omega}{2} \sum_\ell \left[ P_\ell^2 + q_\ell^2 + \sum_{n \geq 2} c_{2n} q_\ell^{2n} \right], \quad [q_\ell, P_\ell] = i. \quad (14)$$

Here,  $P_\ell$  and  $q_\ell$  are the dimensionless momentum and coordinate, respectively. This phonon mode corresponds to the intruded displacement of two opposite carbons perpendicular to the layers. We also take anharmonicity of the phonon into account by  $\Sigma$  over  $n(\geq 2)$  in equation (14). As already mentioned before,  $H_{e-h}$  is mainly based on the  $2p_\pi$  orbital of carbons in each layer. However, as  $q_\ell$  increases, the inter-layer hybridization between  $2p_\pi$  orbitals gradually occurs, as well as intra- and inter-layer hybridizations between  $2s$  and  $2p_\pi$  orbitals. The anharmonicity in equation (14) denotes this hybridization effect phenomenologically. These parameters  $\omega$  and  $c_{2n}$  are determined from equation (7) as,  $\omega = 9.847 \times 10^{-2}$  eV,  $c_4 = -9.280 \times 10^{-4}$  eV,  $c_6 = 1.683 \times 10^{-5}$  eV,  $c_8 = -1.134 \times 10^{-7}$  eV,  $c_{10} = 2.417 \times 10^{-10}$  eV.

$H_c$  in equation (10) denotes the inter-layer Coulomb attraction between the optically excited electron and the hole, and is given by

$$H_c = - \sum_\ell U(q_\ell) [n_{\ell 11} n_{\ell 22} + n_{\ell 12} n_{\ell 21}], \quad n_{\ell ij} \equiv a_{\ell ij}^+ a_{\ell ij}, \quad (15)$$

where  $U(q_\ell)$  is the phonon-dependent Coulomb interaction which is assumed to be linear, as

$$U(q_\ell) = U + U_d q_\ell. \quad (16)$$

Here,  $U = 1.5$  eV and  $U_d = 0.225$  eV, according to the Mataga-Nishimoto formula [65].

Along with the Cho-Toyozawa theory [66], we can define a basis set of our minimal model as a Bloch wave composed of electron-hole-phonon coupled states as,

$$|\Delta, m\rangle = N^{-1/2} \sum_\ell e^{-i\ell k_p} \left[ a_{\ell+\Delta, 11}^+ a_{\ell, 22}^+ \frac{(b_\ell^+)^m}{\sqrt{m!}} \right] |0\rangle, \quad (17)$$

$$k_p \rightarrow 0, \quad b_\ell^+ \equiv \frac{1}{\sqrt{2}}(q_\ell - iP_\ell),$$

where  $\Delta$  denotes a 2-d position vector of the electron relative to the hole created at the  $\ell$ th site, and  $m$  is the number of phonons at the same site.  $|0\rangle$  denotes the electron-hole-phonon vacuum.  $k_p$  is the wave vector of photon which

creates this excitation and  $k_p \rightarrow 0$  as mentioned before. Hence the electron-hole-phonon coupled state generated by visible photons has full translational symmetry just same to that of the lattice. As seen from the above equation, we have taken only the CT excitation to the first layer from the second. We also have assumed that the phonon number  $m$  can become non-zero only when the electron and the hole are in the same site spanning two layers, that is,  $\Delta$  is zero. Since this  $\Delta$  runs all over the 2-d lattice sites, however, equation (17) can describe a largely distant free electron-hole pair, as well as an exciton heavily dressed in  $m(\gg 1)$  phonons.

Using this basis set, we can calculate the matrix elements  $\langle \Delta, m | H | \Delta', m' \rangle$  of the Hamiltonian. Thus, we can perform our calculations, and can get the eigen-state ( $\equiv |w\rangle$ )s and the corresponding eigen-value ( $\equiv E_w$ )s of  $H$ . Using them, we can calculate the early-time dynamics. As an initial state of this time evolution, we can take an exciton wave packet  $|0, 0\rangle$ , instantaneously created by a femto-second photon pulse at time ( $\equiv t$ ) zero, and can calculate the probability ( $\equiv n_{ex}$ ) that it remains in the same state even after a time  $t$  as,

$$n_{ex}(t) = \sum_{w, w'} \langle 0, 0 | w \rangle \left[ \sum_m \langle w | 0, m \rangle \langle 0, m | w' \rangle \right] \times \langle w' | 0, 0 \rangle e^{-it(E_w - E_{w'})}, \quad (18)$$

together with the average phonon number ( $\equiv n_{ph}$ ) of this state, which is defined by

$$n_{ph}(t) = \frac{1}{n_{ex}(t)} \sum_{w, w'} \langle 0, 0 | w \rangle \left[ \sum_m \langle w | 0, m \rangle m \langle 0, m | w' \rangle \right] \times \langle w' | 0, 0 \rangle e^{-it(E_w - E_{w'})}. \quad (19)$$

The energy of this initial state  $|0, 0\rangle$ , being not an eigen-value of  $H$ , is about 3.3 eV with the mean width of about 1.8 eV. Thus, this initial state corresponds to the femto-second pulse excitation by a few visible photons, and its time-evolution is shown in Figure 14 [67] as functions of  $t(2\pi/\omega)$ .

We can see that  $n_{ex}$  rapidly decreases from 1 to about 0.02 within a few femto-second, and becomes rather stable around this value, while  $n_{ph}$  rapidly increases simultaneously. This early-time decrease of  $n_{ex}$  from 1 to about 0.02 is nothing but the free carrier type relaxation, (or the quantum diffusion in the relative space spanned by  $\Delta$ ), as described in Figure 10, and it is the most predominant one, being the characteristic of the good electric conductor. While the residual part 0.02 is nothing but the self-localized exciton.

Once this branching occurs, these two channels are completely separated with each other, and can never be mixed up again, since the exciton has heavily dressed in phonons, while the free carriers are almost bare. When this heavily dressed electron-hole pair tries to move even to a neighboring site, it has to annihilate all these phonons and has to make them again at the neighboring site newly. This probability (quantum coherency) is almost zero. It

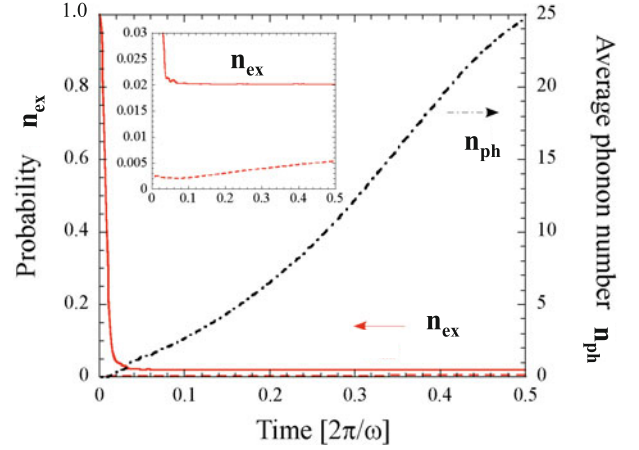


**Fig. 14.**  $n_{ex}$  (solid line) and  $n_{ph}$  (dashed-dotted line) as a function of time  $t(2\pi/\omega)$ . The dashed line, quite close to the horizontal axis, corresponds to the pico-second pulse excitation. The inset shows the close up for  $n_{ex}$ . From reference [67].

is nothing but the spontaneous translational symmetry breaking, and finally makes a classical and local picture for exciton valid.

For comparison, we have also calculated  $n_{ex}$ , taking a largely distant electron-hole pair  $|\Delta, 0\rangle$ , ( $|\Delta| \gg 1$ ) as an initial state, instead of the previous  $|0, 0\rangle$  in equation (18), and its result is also shown in Figure 14, by a dashed line. It is quite close to the horizontal axis in Figure 14, and roughly corresponds, not to the femto-second, but to the pico-second pulse excitation case. We can see almost no self-localized exciton in this case.

## 6.5 Inter-layer $sp^3$ bond formation dynamics

Now, we have already seen the quantum logic of the self-localization. It is often misunderstood to be a sudden shrinkage of the excitation energy or the excitation wave function from the infinitely extended Bloch state to the localized state within a lattice site, for example, localized at the origin of the crystal. This picture of sudden shrinkage is, however, completely wrong and also against the general law of the special relativity that no motion can be faster than the light velocity. Before, during and even after the self-localization, the wave function never shrinks. Its square (the probability density of the excitation at each lattice site of the crystal) is always inversely proportional to  $N$  (volume) of the crystal, being normalized to be one within the whole crystal.

The difference between the extended Bloch state and the localized state occurs only in the presence or the absence of the inter-site quantum phase coherence. The quantum phase coherence between the sites is almost 100% before the self-localization, while it becomes zero after the self-localization. In this stage, all the sites are quantum statistically independent and entirely equivalent. Thus, as the representative of all the sites, we can assume that the electron-hole pair is localized only at a site,

that is, at the origin of the crystal, and can be treated classically.

What we finally obtain, after this self-localization, is the two carbons spanning two layers, largely displaced into the inside between the two layers. These two carbons have a large kinetic energy or a velocity toward the inside of the two layers. While, the electron and the hole are localized around these two carbons, and are almost overlapped with each other, and hence, these two carbons are almost neutral. Thus, the presence of localized exciton gives no serious effect in this final stage. It is quite in contrast to the starting Franck-Condon state, wherein the presence of exciton has given quite important effects.

In this final stage, we can approximately replace the whole state by the classical motion of a graphite type carbon cluster, whose initial condition is the aforementioned inward displacement and velocity of the central two carbons. The original energy donated at the Franck-Condon excitation is now converted into the distortion and the velocity. Although the probability of the self-localization is fractional, the energy conservation law exactly holds even for this fractional component. However, because of the quantum uncertainty, these classical initial conditions should also reflect a large uncertainty  $\pm 1.8$  eV around the given Frank-Condon energy 3.3 eV. Some part of them will be subsequently dissipated into surrounding carbons as ordinary phonons, but some part will surely remain as the stable inter-layer  $\sigma$ -bond.

In this section, by using a classical molecular dynamics (MD), we will see how the inter-layer bond is formed at around the self-localized site. Here, we can also adopt the semi-empirical Brenner potential in this MD. Typical results of this MD calculation [67] are shown Figure 15. As an initial condition, we can give the two opposite carbons an initial distortion (potential energy) and an initial kinetic energy. We can also assume that the initial displacements and initial velocities of the two carbons are in opposite direction, but have the same magnitude. This initial kinetic energy ( $\equiv K_0$ ) is given by  $K_0 = 2(m_c v_0^2/2)$ , where  $m_c$  is the mass of a carbon atom and  $v_0$  is the initial velocity. The initial potential energy is obtained from the relation between the intrusion and the potential energy calculated by using the Brenner's theory [52].

As an example for the case that the inter-layer bond is successfully formed, we show the result for the initial condition that  $K_0 = 3.2$  eV, and the potential energy is 1.54 eV, which corresponds to the initial intrusion of 0.4 Å. Figure 15b shows the snapshots of the MD calculation at times, 0, 0.025, 0.075 and 1.0 ps, where we can see that the inter-layer bond is formed at 1 pico-second. In Figure 15a, we show the time development of the bond length between the two opposite carbons at the origin as a function of time on a logarithmic scale. The inset shows the same plot from 0 to 0.1 pico-second on a linear scale. The bond length decreases from 2.55 Å, rapidly, and it settles down gradually at about 1.56 Å, repeating vibration. This bond length is almost same to that of the diamond structure (1.54 Å).

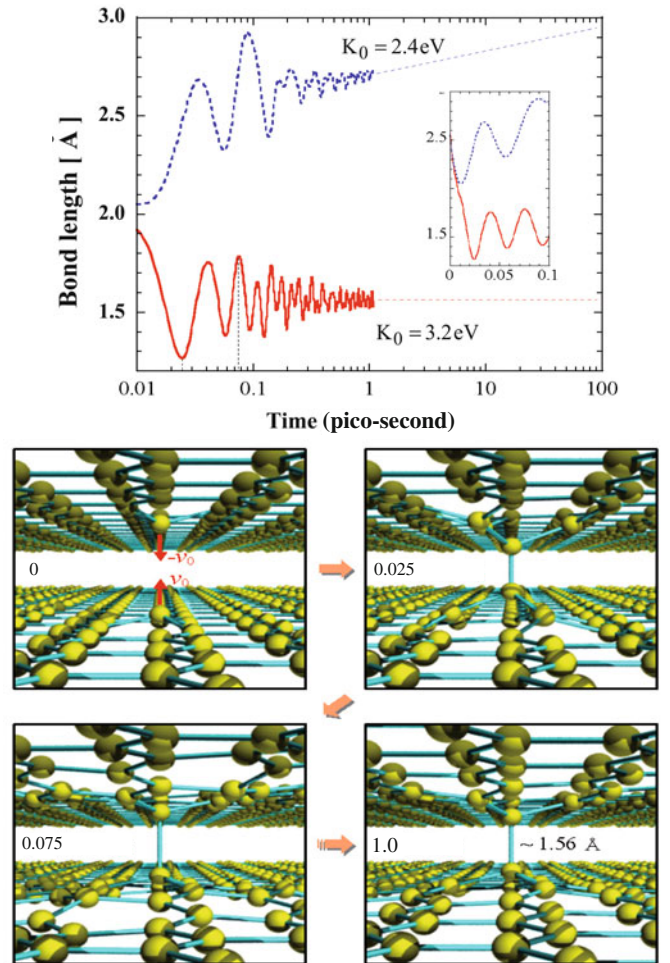


**Fig. 15.** (a) The bond length between the two opposite carbons at the origin as a function of time on a logarithmic scale. The inset shows the same plot from 0 to 0.1 ps on a linear scale. The solid line denotes the case that the initial kinetic energy is 3.2 eV, and the initial intrusion is 0.4 Å. The dashed line is the case that the initial kinetic energy is 2.4 eV with the same initial intrusion. (b) The snapshots of the MD calculation at times, 0, 0.025, 0.075, and 1.0 pico-second. The case that the initial kinetic energy is 3.2 eV and the initial intrusion is 0.4 Å. Only the bonds, whose length is less than 2 Å, are written. From reference [67].

For comparison, by a dashed line in Figure 15a, we have also shown the case of  $K_0 = 2.4$  eV, which does not result in the bond formation. In this case, the system does not overtake the energy barrier to form a bond due to the lack of energy, and returns to the starting graphite without the bond formation. This difference of the failure or the success occurs after the aforementioned self-localization, and hence the final probability to form the stable inter-layer  $sp^3$  bond is about 0.6%.

When the kinetic energy  $K_0$  is much larger than this successful case, as also shown by Nishioka [67], the two carbons once surely contract, but after that, they turn to depart away with each other, because of the too much excess kinetic energy. This result closely relates to the recent

experiment by Carbone [68], wherein the inter-layer contraction transiently induced by the photo-irradiation, is soon followed by the ablation.

## 7 Summary and supplementation

Thus, we have reviewed the various photo-induced structural phase transitions. The starting assumption shown in Figure 1 is that, we have our true ground state, which is absolutely stable, or its lifetime is infinitely long. Shining a few visible photons on to it, we can get a macroscopic photo-induced phase. This photo-induced phase can be an entirely new one different from any other existing equilibrium phases. In some case, this photo-induced phase may have a longer lifetime even as compared with the time scale of our daily life.

Incidentally, let us briefly see the other type of PSPT not mentioned above. In Figure 1, we have tacitly assumed the system evolves along the potential surface of the excited state after the photo-excitation, or the excited electron and the induced lattice distortion (or phonons) always evolve together. However, the excited electron can also release a quite large amount of phonons during the lattice relaxation as seen from Figure 1. If such released phonons can become entirely independent of the original electron, and also can be superposed coherently with each other all over the crystal, they result in another PSPT. They have very large amplitudes than the ordinary thermal phonons. Hence, they can overcome the energy barrier in the ground state potential surface shown in Figure 1, and can go into a new phase. This type PSPT, or the so-called non-thermal melting, along the ground state potential surface is also a quite interesting phenomenon, as shown by Sokolowski-Tinten [69].

This work is supported by the Ministry of Education, Culture, Sports, Science and Technology of Japan, the peta-computing project, and Grant-in-Aid for Scientific Research (S), Contract No. 19001002, 2007.

## References

1. J. Ziman, *Models of Disorder* (Cambridge, London, 1979)
2. M. Ueta, H. Kanzaki, H. Kobayashi, H. Toyozawa, E. Hanamura, *Excitonic Processes in Solids* (Springer, Berlin, 1986), p. 203
3. K. Nasu, Report on Progress in Physics **67**, 1607 (2004)
4. K. Nasu, *Photo-induced phase transitions* (World Scientific, Singapore, 2004)
5. K. Yonemitsu, K. Nasu, Phys. Rep. **465**, 1 (2008)
6. S. Koshihara, J. Phys. Conf. Ser. **148**, 01101 (2009), and other papers in this volume
7. C. Kittel, *Introduction to Solid State Physics*, 7th edn. (John Wiley, New York, 1996), p. 53
8. Y. Tokura, T. Koda, T. Mitani, G. Saito, Solid State Commun. **43**, 757 (1982)
9. S. Koshihara, H. Takahashi, H. Sakai, Y. Tokura, T. Luty, J. Phys. Chem. B **103**, 2592 (1999)
10. T. Suzuki, T. Sakamaki, K. Tanimura, S. Koshihara, Y. Tokura, Phys. Rev. B **60**, 6191 (1999)
11. J. Thompson, H. Stewart, *Nonlinear Dynamics and Chaos* (John Wiley, New York, 2002), p. 3
12. H. Mizouchi, K. Nasu, J. Phys. Soc. Jpn **70**, 2175 (2001)
13. R. Yabuki, K. Nasu, Phys. Lett. A **320**, 286 (2004)
14. S. Iwai, S. Tanaka, K. Fujinuma, H. Kishida, H. Okamoto, Y. Tokura, Phys. Rev. Lett. **88**, 057402 (2002)
15. H. Okamoto, Y. Ishige, S. Tanaka, H. Kishida, S. Iwai, Y. Tokura, Phys. Rev. B **70**, 165202 (2004)
16. J. Polanyi, W. Wong, J. Chem. Phys. **51**, 1439 (1969)
17. M. Child, *Molecular Collision Theory* (Academic Press, London, 1974), p. 217
18. L. Luer, C. Manzoni, G. Cerullo, G. Lanzani, M. Meneghetti, Phys. Rev. Lett. **99**, 027401 (2007)
19. I. Katayama, T. Kon, K. Mitarai, J. Takeda, Phys. Rev. B **80**, 092103 (2009)
20. T. Nishihara, M. Nihei, H. Oshio, K. Tanaka, J. Phys. Conference Series **148**, 012033 (2009)
21. D. Glijer, J. Hébert, E. Trzop, E. Collet, L. Toupet, H. Cailleau, G. Matouzenko, H. Lazar, J. Létard, S. Koshihara, M. Buron-Le Cointe, Phys. Rev. B **78**, 134112 (2008)
22. Y. Takahashi, H. Kitagawa, T. Suemoto, Phys. Rev. B **79**, 153103 (2009)
23. O. Sato, T. Iyoda, A. Fujishima, K. Hashimoto, Science **272**, 704 (1996)
24. X. Liu, Y. Moritomo, A. Machida, A. Nakamura, H. Tanaka, T. Kawai, Phys. Rev. B **63**, 115105 (2001)
25. P. Baum, D. Yang, A. Zewail, Science **318**, 788 (2007)
26. L. Perfetti, P. Loukakos, M. Lisowski, U. Bovensiepen, M. Wolf, H. Berger, S. Biermann, A. Georges, New J. Phys. **10**, 053019 (2008)
27. F. Daniele, O. Misochko, P. Loosdrecht, Phys. Rev. B **80**, 161207 (2009)
28. H. Tokoro, S. Ohkoshi, K. Hashimoto, Appl. Phys. Lett. **82**, 1245 (2003)
29. Y. Qiu, C.Q. Wu, K. Nasu, Phys. Rev. B **72**, 224105 (2005)
30. Y. Yamada, K. Tanaka, J. Phys. Soc. Jpn **77**, 054704 (2008)
31. K. Miyano, T. Tanaka, Y. Tomioka, Y. Tokura, Phys. Rev. Lett. **78**, 4257 (1997)
32. N. Tajima, J. Fujisawa, N. Naka, T. Ishihara, R. Kato, Y. Nishio, K. Kajita, J. Phys. Soc. Jpn **74**, 511 (2005)
33. Y. Okimoto, X. Peng, M. Tamura, T. Morita, K. Onda, T. Ishikawa, S. Koshihara, N. Todoroki, T. Kyomen, M. Itoh, Phys. Rev. Lett. **103**, 027402 (2009)
34. C. Siders, A. Cavalleri, Science **300**, 591 (2003)
35. E. Collet, M. Cailleau, M. Cointe, H. Cailleau, M. Wulff, T. Luty, S. Koshihara, M. Meyer, L. Toupet, P. Rabiller, S. Techert, Science **300**, 612 (2003)
36. J. Kanasaki, E. Inami, K. Tanimura, H. Ohnishi, K. Nasu, Phys. Rev. Lett. **102**, 087402 (2009)
37. R. Raman, Y. Murooka, C. Ruan, T. Yang, S. Berber, D. Tomanek, Phys. Rev. Lett. **101**, 077401 (2008)
38. Y. Toyozawa, J. Phys. Soc. Jpn **58**, 2626 (1989)
39. Y. Shinozuka, Y. Toyozawa, J. Phys. Soc. Jpn **46**, 505 (1979)
40. E. Hanamura, N. Nagaosa, J. Phys. Soc. Jpn **56**, 2080 (1987)
41. K. Koshino, T. Ogawa, J. Phys. Soc. Jpn **67**, 2174 (1998)
42. K. Ishida, K. Nasu, Phys. Rev. Lett. **100**, 116403 (2008)
43. T. Sakano, Y. Toyozawa, J. Phys. Soc. Jpn **65**, 671 (1996)

44. P. Huai, H. Zheng, K. Nasu, J. Phys. Soc. Jpn **69**, 1788 (2000)
45. A. Takahashi, H. Itoh, M. Aihara, Phys. Rev. B **77**, 205105 (2008)
46. H. Matsueda, S. Ishihara, J. Phys. Soc. Jpn **76**, 083703 (2007)
47. K. Iwano, Phys. Rev. Lett. **102**, 106405 (2009)
48. N. Tsuji, T. Oka, H. Aoki, Phys. Rev. B **77**, 205105 (2008)
49. F. Bundy, J. Chem. Phys. **38**, 631 (1963)
50. F. Banhart, J. Appl. Phys. **81**, 3440 (1997)
51. H. Nakayama, H. Yoshida, J. Phys. CM **15**, R1077 (2003)
52. D. Brenner, Phys. Rev. B **42**, 9458 (1990)
53. S. Fahy, S. Louise, M. Cohen, Phys. Rev. B **34**, 1191 (1986)
54. S. Fahy, S. Louise, M. Cohen, Phys. Rev. B **35**, 7623 (1987)
55. Y. Tateyama, T. Ogitsu, K. Kusakabe, S. Tsuneyuki, Phys. Rev. B **54**, 14994 (1996)
56. I. Shirotni, J. Hayashi, K. Takeda, H. Kawamura, M. Inokuchi, K. Yakushi, H. Inokuchi, Mol. Cryst. Liq. Cryst. **461**, 93 (2007)
57. H. Ohnishi, K. Nasu, Phys. Rev. B **80**, 0141121 (2009)
58. Research highlights, Nature (London) **458**, 129 (2009)
59. H. Ohnishi, K. Nasu, Phys. Rev. B **79**, 054111 (2009)
60. J. Slater, G. Koster, Phys. Rev. **94**, 1498 (1954)
61. W. Harrison, *Electronic Structure and the Properties of Solids* (Freeman, San Francisco, 1980), p. 27
62. L. Radosinski, K. Nasu, J. Kanazaki, K. Tanimura, A. Radosz, T. Luty, *Molecular Electronic and Related Materials-Control and Probe with Light* (Transworld Research Network, Trivandrum, 2010), p. 281
63. A. Bianconi, S. Hagstrom, R. Bachrach, Phys. Rev. B **16**, 5543 (1977)
64. H. Nishimoto, T. Nakatani, T. Matsushita, S. Imada, H. Daimon, S. Suga, J. Phys. CM **8**, 2715 (1996)
65. N. Mataga, K. Nishimoto, Z. Phys. Chem., Neue Folge **13**, 140 (1981)
66. K. Cho, Y. Toyozawa, J. Phys. Soc. Jpn **30**, 1555 (1971)
67. K. Nishioka, K. Nasu, Phys. Rev. B **80**, 235420 (2009)
68. F. Carbone, P. Baum, P. Rudolf, A. Zewail, Phys. Rev. Lett. **100**, 035501 (2008)
69. K. Sokolowski-Tinten, C. Blome, J. Blums, A. Cavalleri, C. Dietrich, A. Tarasevitch, I. Uschman, E. Forster, M. Kammler, M. Horn-von-Hoegen, D. von der Linde, Nature **422**, 287 (2003)